JOURNAL OF CATALYSIS 88, 54–64 (1984)

Structure and Activity of NiO/α-Al_2O_3 and NiO/ZrO_2 Calcined at High Temperatures

I. Structure

G. R. GAVALAS,* C. PHICHITKUL,* AND G. E. VOECKS†

*Division of Chemistry and Chemical Engineering and †Jet Propulsion Laboratory, California Institute of Technology, Pasadena, California 91125

Received December 13, 1982; revised February 14, 1984

A series of NiO/α-Al_2O_3 and NiO/ZrO_2 catalysts were prepared by impregnation and calcination in air between 750 and 1050°C. Examination of the catalysts by means of nitrogen adsorption, H_2 chemisorption, X-ray diffraction, scanning electron microscopy, and X-ray photoelectron spectroscopy showed marked variations in physical and chemical properties as a function of calcination temperature. The results indicate that NiO does not interact with ZrO_2 whereas NiO–Al_2O_3 interaction is extensive at the interface between NiO and Al_2O_3 when the calcination temperature exceeds 850°C. When the calcined samples of NiO/ZrO_2 were reduced in hydrogen, extensive redispersion of the metal was observed.

INTRODUCTION

The chemical and physical structure of supported nickel catalysts has been the subject of many investigations. Several of these have concentrated on the interaction between nickel oxide and support, especially alumina support. This interaction depends on nickel loading and calcination temperature and has been attributed to the formation of nickel aluminate spinel (*1–5*) or to nickel ions in tetrahedral and octahedral sites of γ-alumina (*6*) or to "modification" of the electronic properties of nickel oxide due to interaction with alumina (*7*). These conclusions are not necessarily incompatible since the area, depth, and crystalline nature of any compound formed between nickel oxide and alumina varies with conditions of preparation (e.g., coprecipitation vs impregnation conditions) and calcination. Nickel–support interaction has been found to have an important effect on oxide reducibility (*1, 8–11*) and catalytic activity (*9–11*). The effect of calcination temperature on physical properties such as surface area and crystallite size distribution has been dealt with in Ref. (*12*).

In the present paper (Part I) we report results concerning the chemical state and the surface area of supported nickel subjected to various thermal pretreatments and reduction–oxidation cycles. Unlike previous studies which employed support materials of high surface area such as γ- or η-alumina and silica, we have employed α-alumina and zirconia supports, both of low surface area. Because of the less facile interaction between the support and the nickel oxide, it has been possible to employ higher calcination temperatures and observe rather unusual effects of calcination temperature on the nickel surface area. In the following paper (Part II) we report results about the reactivity of these supported nickel catalysts with respect to the partial oxidation of methane. The reactivity studies concentrate on catalysts which are initially in the oxide form.

Partial oxidation and steam reforming of hydrocarbons on supported nickel has been reviewed relative to industrial applications

0021-9517/84 $3.00

TABLE 1

Properties of Supports

Support	Crystalline compound	Total surface area (m^2/g)	Pore volume (cm^3/g)
Alcoa T-61 α-Al_2O_3	α-Al_2O_3	0.10	0.015
Norton SZ5464 ZrO_2	ZrO_2	0.40	0.20

in Ref. (*13*) and relative to catalyst structure and reaction mechanism in Refs. (*10, 11*). Depending on the steam-to-hydrocarbon or oxygen-to-hydrocarbon ratio, the nickel exists either in the metallic or the oxide form. In either case the reactions require relatively high temperatures, above 600°C, which pose problems concerning nickel–support interactions, and deactivation by loss of surface area or loss of specific activity.

EXPERIMENTAL

1. Preparation. Two commercially available supports with properties as shown in Table 1 were crushed and screened to 60–80 mesh and then impregnated with 2-*M* $Ni(NO_3)_2$ solution at room temperature. After 15 min of impregnation, the solution was decanted and the sample was filtered and dried at 80–100°C for 24 h. The sample was then heated in air at 400°C for 1 h to decompose the $Ni(NO_3)_2$. This procedure was repeated several times to obtain the desirable nickel loading. Those catalysts which were not heated above 400°C were labeled as "noncalcined." Subsequent heating in air at 750 to 1050°C of the noncalcined catalysts provided the calcined catalyst samples.

2. Wet chemical analysis. The amount of nickel in oxide form was determined by acidic extraction of nickel from the support followed by dimethylglyoxime precipitation (*7*). The first step in the chemical analysis was to dissolve the NiO in 5 *N* HCl. It has been shown in our laboratory that nickel contained as $NiAl_2O_4$ is not extracted by this method. Hence, the difference in the nickel content before and after the high temperature calcination provides the amount of the $NiAl_2O_4$ component. For comparison purposes, similar analyses were carried out for the zirconia-supported catalysts.

3. Total and nickel surface areas. Both were measured by Pacific Sorption Service using a static gas absorption apparatus. Total surface area was measured by N_2 adsorption. The data were interpreted using the BET equation and an effective cross-sectional area of 16.2 $Å^2$ for N_2.

The nickel surface area was measured by H_2 chemisorption at 0°C. Prior to chemisorption the samples were reduced in hydrogen for 2 h at 500°C. The results were obtained in micromoles of hydrogen per gram of sample and were converted to square meters per gram of sample using the stoichiometry 6.77×10^{-2} nm^2/atom (*14*). This stoichiometry is based on the assumption of one hydrogen atom per surface nickel atom and an equal distribution of the three lowest index planes of nickel (fcc).

4. X-Ray diffraction. Identification of crystalline compounds and determination of average crystallite size were carried out by X-ray diffraction (XRD) using a G.E. diffractometer with Ni filter and Cu$K\alpha$ radiation.

The mean crystallite size (D) is related to the pure X-ray broadening (β) by the Scherrer formula

$$D = K\lambda/\beta \cos \theta.$$

The size (D) was defined as $(\text{volume})^{1/3}$ leading to a value $K \simeq 0.95$ (*15, 16*) when β is defined as the half-maximum linewidth. The half-maximum linewidth from NiO (220) and NiO(111) reflecting planes were employed for the alumina-supported and zirconia-supported catalysts, respectively. The instrumental line broadening was determined from the half-maximum linewidth of a single silicon crystal.

5. SEM studies. The catalysts were examined in an AMR 900 scanning electron microscope with resolution of about 500–1000 Å. The samples were coated with gold

TABLE 2

Properties of the $NiAl_2O_4$ Standard

Support	T-375 α-Al_2O_3
Ni %[a]	17.3
Calcination conditions	1370°C, 50 h
Total surface area	2.37 m^2/g
Average crystallite size of $NiAl_2O_4$	630 Å
Crystalline compound (XRD)	$NiAl_2O_4$, α-Al_2O_3
Color	Blue

[a] Chemical analysis prior to calcination.

to about 100–200 Å thickness prior to observation.

6. X-Ray photoelectron spectroscopy (XPS). Photoelectron spectra were obtained using a HP 5950 B spectrometer. The sample chamber was pumped to a pressure of 5×10^{-9} Torr and monochromatized Al$K\alpha$ exciting radiation was used.

All samples were dusted onto a double-sided adhesive taped on a gold-plated copper sample holder. The electron binding energies for the Ni($2p_{3/2}$), O(1*s*), and Al(2*p*) were recorded and compared with those for the NiO and $NiAl_2O_4$ standards. Since the standards and the catalysts charged to 1–3 eV due to their insulating nature, the displacement of the binding energy of the contaminant C(1*s*) peak from a standard value of 284.6 eV was used for correction.

The NiO standard was a commercially available, high purity powder (Ventron Corp. 99.99% purity). The $NiAl_2O_4$ standard was prepared by calcination of the noncalcined NiO/T-375 α-Al_2O_3 sample in air at 1370°C for 50 h. After calcination, the XRD spectrum and the chemical analysis showed $NiAl_2O_4$ to be the only nickel compound present in the sample. The properties of the $NiAl_2O_4$ standard are shown in Table 2.

RESULTS

1. XRD and Wet Chemical Analyses

Tables 3–6 list the properties of supported catalysts subjected to different calcination pretreatments. Wet chemical analyses of all zirconia-supported samples showed the same nickel content before and after calcination. Examination of the XRD spectra showed no lines characteristic of a nickel–zirconium compound such as the zirconium nickel oxide $Zr_{0.67}Ni_{0.22}O_{0.11}$. Rather different results were observed for the alumina-supported catalysts. The XRD spectra did not contain lines characteristic of $NiAl_2O_4$. However, wet chemical analyses of the samples NiO/α-Al_2O_3-950 and NiO/α-Al_2O_3-1050 showed that a significant fraction of nickel oxide reacted with the support to form a nickel species insoluble in the acid. The extent of this reaction increased with the temperature of calcination.

The average crystallite size estimated from X-ray line broadening for NiO on both the NiO/α-Al_2O_3 and NiO/ZrO_2 samples is

TABLE 3

Properties of Zirconia-Supported Catalysts

Catalyst designation	Ni(wt%) prior to calcination	Calcination in air	Ni(wt%) after calcination	D^a_{NiO} (Å)	Crystalline compounds (XRD)	Color
NiO/ZrO_2 (noncalcined)	6.6	None	6.6	440	NiO, ZrO_2	Black
NiO/ZrO_2-750	6.6	750°C, 15 h	6.6	440	NiO, ZrO_2	Gray
NiO/ZrO_2-850	6.6	850°C, 15 h	6.6	440	NiO, ZrO_2	Gray
NiO/ZrO_2-950	6.6	950°C, 15 h	6.6	440	NiO, ZrO_2	Gray
NiO/ZrO_2-1050	6.6	1050°C, 15 h	6.6	440	NiO, ZrO_2	Grayish yellow

[a] Average crystallite size estimated from X-ray line broadening.

TABLE 4

Physical Properties of Alumina-Supported Catalysts

Catalyst designation	Ni(wt%) prior to calcination	Calcination in air	Ni(wt%) after calcination	D^a_{Nio} (Å)	Crystalline compounds (XRD)	Color
NiO/α-Al_2O_3 (noncalcined)	2.20	None	2.20	300	NiO, α-Al_2O_3	Black
NiO/α-Al_2O_3-750	2.20	750°C, 2 h	2.20	300	NiO, α-Al_2O_3	Gray
NiO/α-Al_2O_3-850	2.20	850°C, 3 h	2.20	300	NiO, α-Al_2O_3	Gray
NiO/α-Al_2O_3-950	2.20	950°C, 15 h	1.54	290	NiO, α-Al_2O_3	Green
NiO/α-Al_2O_3-1050	2.20	1050°C, 15 h	1.29	290	NiO, α-Al_2O_3	Greenish blue

[a] Average crystallite size estimated from X-ray line broadening.

seen to be independent of the calcination procedure. A slight decline in the average crystallite size of NiO is observed in the NiO/α-Al_2O_3-950 and NiO/α-Al_2O_3-1050 catalysts for which the interaction with the support was found to be extensive from wet chemical analyses.

2. *Surface Areas*

Table 5 lists the nickel and total surface areas of Ni/ZrO_2 catalysts prepared at different calcination temperatures. The measurements were subject to an error of about ± 0.05 m^2/g. Unfortunately the size of the Ni/Al_2O_3 samples was inadequate for meaningful measurements given the extremely small surface area of the alumina support.

The nickel surface area of calcined Ni/ZrO_2 first decreases and then increases with calcination temperature, exhibiting a minimum at about 850°C. The total surface area of the (oxidized) NiO/ZrO_2 samples is subject to considerable scatter but seems to decrease with calcination temperature. The total surface area of the reduced samples shows a similar effect of calcination temperature as the nickel area. It first decreases and then increases as the calcination temperature exceeds 850°C. In all samples the total surface area is significantly higher after reduction.

TABLE 5

Ni and Total Surface Areas of Zirconia-Supported Catalysts

Catalyst	Ni surface area (m^2/g)	Total surface area (m^2/g)	
		Before reduction	After reduction
NiO/ZrO_2 noncalcined	0.64	0.93	1.10
NiO/ZrO_2-750	0.38	0.85	0.93
NiO/ZrO_2-850	0.32	0.68	0.89
NiO/ZrO_2-950	0.56	0.80	1.31
NiO/ZrO_2-1050	0.66	0.61	1.26

3. *Catalyst Color*

The noncalcined NiO/ZrO_2 catalyst is black. After calcination between 750 and 950°C, the catalyst becomes gray, and a grayish yellow catalyst is obtained at 1050°C. Similarly, the noncalcined NiO/α-Al_2O_3 catalyst is black. After calcination at 750 and 850°C, the catalyst becomes gray. However, after calcination at 950 and 1050°C, the color changes and becomes green to greenish blue. These catalysts were kept in air at room temperature for several months without any change in color. As indicated earlier, after reduction in H_2 at 450°C and reoxidation in air at 500°C all catalysts become black.

4. *SEM Results*

Figures 1–4 are electron micrographs of the alumina support and the supported nickel samples NiO/α-Al_2O_3 750, 850, and 1050. A comparison of the α-Al_2O_3 and the NiO/α-Al_2O_3 samples indicates that the latter involves extensive coverage by NiO

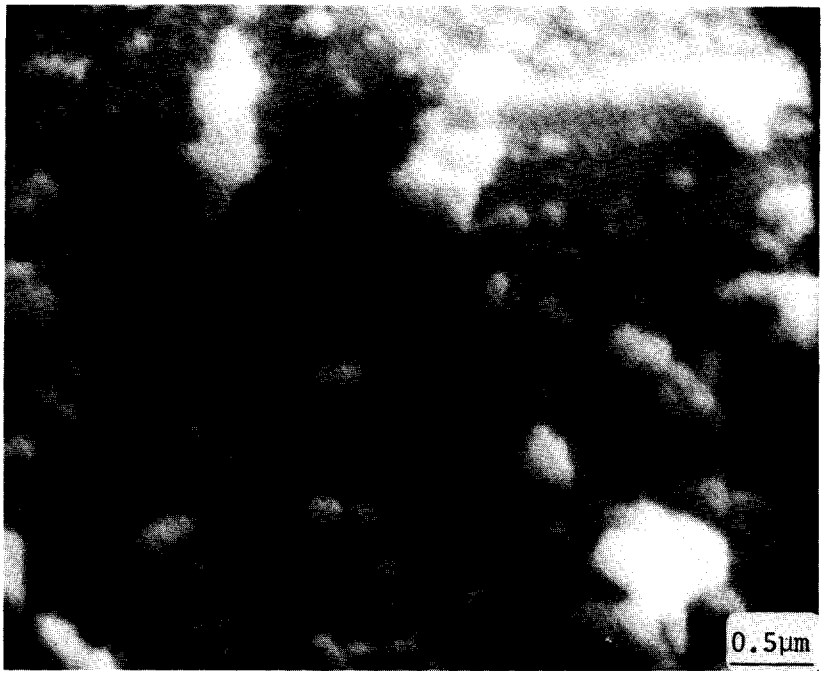

FIG. 1. Scanning electron micrograph of α-Al_2O_3 at $\times$20,000.

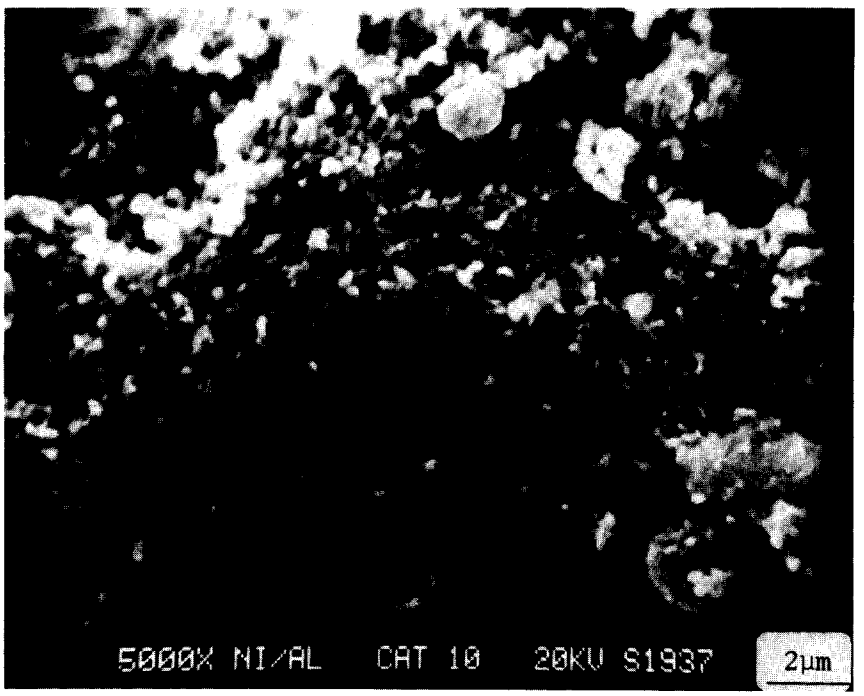

FIG. 2. Scanning electron micrograph of NiO/α-Al_2O_3-750 at $\times$5000.

FIG. 3. Scanning electron micrograph of NiO/α-Al_2O_3-850 at ×5000.

FIG. 4. Scanning electron micrograph of NiO/α-Al_2O_3-1050 at ×20,000.

TABLE 6

Surface Elemental Composition (%)

Sample	Ni	Al	O	C	Na	Ca	Ti	Cl	Ni/Al
NiO	33	—	43	23	—	—	—	1.2	—
$NiAl_2O_4$	4.0	24	52	19	—	—	0.2	—	0.17
NiO/α-Al_2O_3-850	24	~14	42	20	—	—	—	—	~1.71
NiO/α-Al_2O_3-1050	15	15	48	21	0.9	0.5	—	—	1.00
NiO/α-Al_2O_3-1050 (NiO extracted)	8.9	21	51	18	1.1	—	—	—	0.42

Note. —: Absence of signal, ~: approximate value.

particles in the size range 1000–2000 Å. This size is much larger than the crystallite size of 300 Å estimated from X-ray line broadening. Moreover, the NiO particle size does not seem to vary with calcination temperature except that the particles in the sample calcined at 1050°C seem somewhat smoother.

5. *XPS Results*

XPS was applied to the samples NiO/α-Al_2O_3-850 and NiO/α-Al_2O_3-1050. To test for the presence of $NiAl_2O_4$, a sample of NiO/α-Al_2O_3-1050 from which NiO was removed by dilute hydrochloric acid was also examined. The surface elemental composition of various samples is listed in Table 6. The results show only Ni, O, and Al for the NiO/α-Al_2O_3-850 sample and additional traces of Ca and Na for the NiO/α-Al_2O_3-1050 sample.

TABLE 7

Electron Binding Energies for Standard Samples (eV)

Sample	Ni($2p_{3/2}$)	O(1*s*)	Al(2*p*)	ΔE
NiO	854.4[a]	529.4[a]	—	325
	855.7	531.4		
	861.4			
$NiAl_2O_4$	856.7[a]	531.3	74.5	325.4

Note. ΔE: Ni($2p_{3/2}$)–O(1*s*) binding energy separation (principal peaks).

[a] Principal peaks.

The electron binding energies for standards and supported nickel samples are listed in Tables 7 and 8. Figures 5 to 7 show the spectra of the supported samples. The results, corrected according to the C(1*s*) peak position, are described below.

a. NiO standard. The Ni($2p_{3/2}$) spectrum has principal peaks at 854.4 and 855.9 eV and is accompanied by a broad satellite peak at 861.4 eV. The origin of this satellite is still a matter of debate. Wertkeim and Hufner (*17*) have suggested that it is due to the shake-up transition $d^8 \rightarrow d^{8*}$. Kim and Davis (*18*) have suggested that the satellite is due to the exchange interaction of 2*p* and 3*d* electrons. The O(1*s*) spectrum has a principal peak at 529.4 eV and is accompanied by a satellite shoulder at 531.3 eV. The

TABLE 8

Electron Binding Energies (eV)

Sample	Ni($2p_{3/2}$)	O(1*s*)	Al(2*p*)	ΔE
NiO/α-Al_2O_3-850	854.9[a]	530.0[a]	73.5	324.9
	856.5	[b]		
	861.8			
NiO/α-Al_2O_3-1050	855.2[a]	530.4[a]	73.8	324.8
	856.6	[b]		
	861.8			
NiO/α-Al_2O_3-1050 (NiO extracted)	856.1[a]	530.7	73.8	325.4
	862.1			

Note. ΔE: Ni($2p_{3/2}$)–O(1*s*) binding energy separation (principal peaks).

[a] Principal peak.

[b] A broad satellite shoulder.

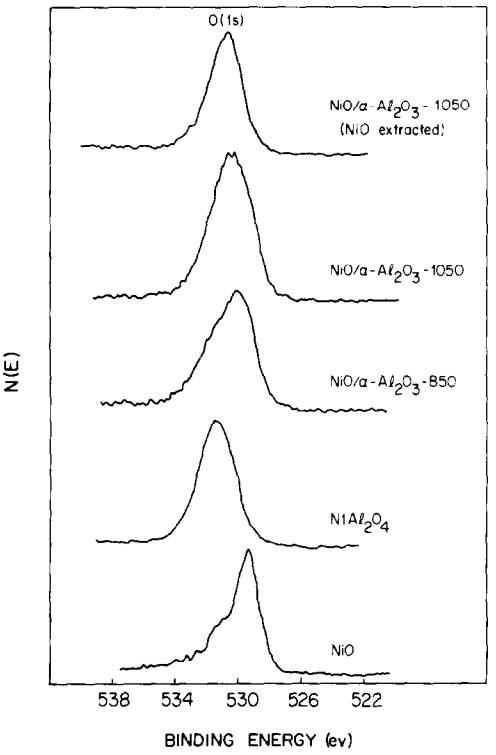

FIG. 5. O(1*s*) core level peak for catalysts and standard samples. Binding energies are corrected for charging by reference to C(1*s*) = 284.6 eV.

spectra are similar to those reported by other investigators (*4, 18–20*).

b. $NiAl_2O_4$ standard. The Ni($2p_{3/2}$) spectrum has a principal peak at 856.7 eV with an accompanying satellite at 863.3 eV. The spectrum of O(1*s*) is also a singlet with binding energy at 531.3 eV. Hence, the Ni($2p_{3/2}$) and O(1*s*) binding energy separation is 0.4 eV higher than that observed for NiO. The Al(2*p*) binding energy is observed at 74.5 eV.

c. NiO/α-Al_2O_3-1050 (NiO extracted). The Ni($2p_{3/2}$) and O(1*s*) spectra are similar to those observed for the $NiAl_2O_4$ standard both in overall line shape and linewidth. However, the Ni($2p_{3/2}$) and O(1*s*) binding energies are 0.6 eV lower than those observed for the $NiAl_2O_4$ standard.

d. NiO/α-Al_2O_3-850 and NiO/α-Al_2O_3-1050. The Ni($2p_{3/2}$) spectra for both catalysts exhibit structural characteristics similar to those observed for NiO. The spectra have broader linewidths compared to those observed for the $NiAl_2O_4$ standard due to an accompanying satellite shoulder. The O(1*s*) spectra also appear quite similar to those observed for NiO, with a broad weak shoulder on the higher binding energy side. Although the observed Ni($2p_{3/2}$) and O(1*s*) peaks for these two catalysts are shifted by about 1 eV higher than those for NiO, their Ni($2p_{3/2}$) and O(1*s*) binding energy separations agree quite well with those of NiO.

DISCUSSION AND CONCLUSIONS

1. Identity of the Nickel Compound

In comparing the present results with those of previous studies one should keep in mind differences in the crystalline phase of the alumina support, in the method of preparation (coprecipitation vs impregna-

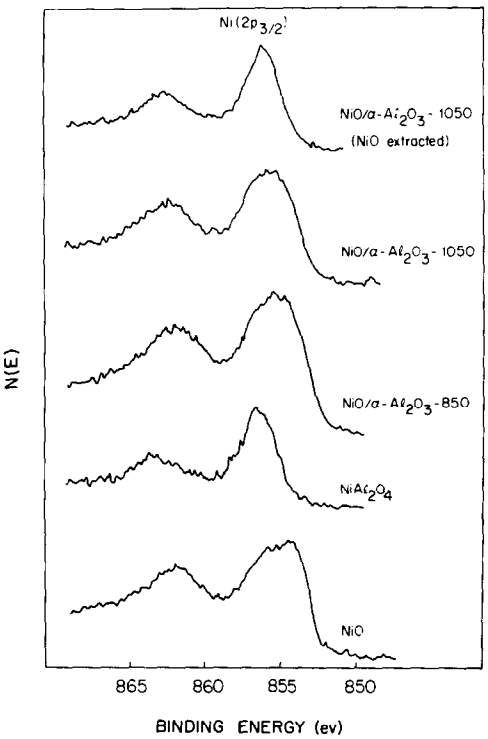

FIG. 6. Ni($2p_{3/2}$) core level peak for catalysts and standard samples. Binding energies are corrected for charging by reference to C(1*s*) = 284.6 eV.

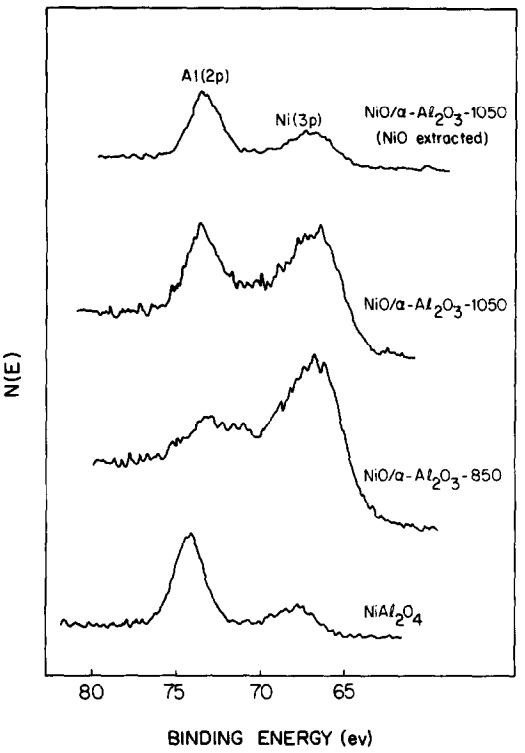

FIG. 7. Al(2*p*) core level peak for catalysts and standard sample. Binding energies are corrected for charging by reference to C(1*s*) = 284.6 eV.

tion), in the temperature of calcination, and in the nickel loading per unit surface area of support.

Vedrine *et al.* (*7*) obtained XPS spectra for various supported NiO materials. One of the materials used was NiO/α-Al_2O_3 with nickel loading 5.4×10^{-4} g/m^2 prepared by impregnation and calcination at 500°C. The observed narrowing of the Ni($2p_{3/2}$) peak and other differences in spectral parameters between NiO/α-Al_2O_3 and pure NiO were attributed to strong electronic interaction with the support or formation of a new Ni species. Wu and Hercules (*6*) examined the XPS spectra of a series of NiO/α-Al_2O_3 samples with nickel loadings in the range 7.8×10^{-4} to 37×10^{-4} g/m^2 prepared by impregnation and calcination at 600°C. The Ni($2p_{3/2}$) peak characteristic of crystalline NiO appeared only at loadings exceeding 26×10^{-4} g/m^2. At lower loadings, NiO was strongly interacting with the support. The width of the Ni($2p_{3/2}$) peak and the reducibility in hydrogen suggested two distinct surface nickel species.

The nickel loading of the NiO/α-Al_2O_3 samples employed in this work was 0.2 g/m^2, several orders of magnitude higher than that employed in the aforementioned studies. The calcination temperature was also higher. As already discussed, the XPS spectrum of the sample calcined at 1050°C and subsequently extracted by acid displays Ni($2p_{3/2}$) and O(1*s*) peaks that have the same shape and separation as the $NiAl_2O_4$ standard, although the absolute binding energies are 0.6 eV lower. The X-ray diffractogram of the acid-extracted sample confirmed complete extraction of NiO but showed no evidence of spinel $NiAl_2O_4$. Thus, the nickel remaining after extraction is not in the form of crystalline spinel, although its bonding environment as evidenced by the shape and separation of the Ni($2p_{3/2}$) and O(1*s*) peaks is very close to that of the bulk spinel sample, which is also not extractable by acid.

In contrast to the acid-extracted sample, the samples calcined at 850 and 1050°C have XPS spectrum with identical shapes and separation for the Ni($2p_{3/2}$), O(1*s*) peaks as the NiO standard (Figs. *5,6*). The binding energy of the Al(2*p*) peak, 73.5 and 73.8 eV in the 850 and 1050°C samples, respectively, is shifted toward but does not reach the 74.5-eV energy peak observed for the standard spinel sample (Fig. 7). The absence of Ni($2p_{3/2}$) and O(1*s*) peak characteristics analogous to those of the acid-extracted sample is evidently due to the presence of the nickel oxide layer, approximately 300-Å thick above the interface with alumina.

2. *Particle Size*

SEM examination of the calcined NiO/α-Al_2O_3 samples has shown most NiO particles to be in the range 1000–2000 Å, much larger than the average crystallite size of 300 Å estimated from X-ray line broaden-

ing. This disparity may be explained in different ways. One possibility is the formation of agglomerates of crystallites sized 1000–2000 Å. Such agglomerates have been observed before, e.g., by Figlarz *et al.* (*21*) for unsupported CoO and by Amelse *et al.* (*24*) for Fe_2O_3/SiO_2. The latter investigators determined the morphology of the agglomerates by transmission electron microscopy and verified that the Scherrer formula provides a somewhat overestimated size of the component crystallites.

A second possibility is the formation of rafts with thickness about 300 Å and diameter 1000–2000 Å. Again, SEM would indicate the diameter while the Scherrer formula would indicate the thickness, 300 Å. Such rafts have been observed by scanning TEM by Wang and Schmidt (*23*) for Rh- and Pt–Rh-supported on thin films of SiO_2 and Al_2O_3. The small thickness of these particles has been attributed to spreading caused by the low interfacial tension between metal oxide and the support material (*23, 24*). The low spatial resolution of our SEM instrument did not allow to determine whether the particles 1000–2000 Å were agglomerates of distinct crystallites as observed in (*21, 22*) or flat disks as observed in (*23*).

3. *Nickel Redispersion*

Inspection of Table 5 shows that the total surface area of the zirconia-supported samples increases significantly with reduction. This increase implies substantial metal redispersion. Furthermore, the metal surface area increases with the temperature of calcination, at least when that temperature exceeds 850°C. These results are similar to Wang and Schmidt's (*23*) results on metal redispersion upon the reduction of the oxide. The explanation advanced by these authors is that the thin metal oxide "rafts" break up into a number of smaller metal particles, possibly because, unlike the oxide, the metal does not wet the support. The present results are consistent with this explanation. The effect of prior calcination temperature could be to increase the spreading of the oxide and thereby increase the number of metal particles formed upon reduction. An alternative explanation also advanced in (*23*), involved the elastic stresses generated upon reduction of the oxide. At higher calcination temperatures the stronger bonding between oxide and support would result in larger stresses and more pronounced fragmentation during reduction.

REFERENCES

1. Ljubarkij, G. D., Ardeeva, L. B., and Kulkova, N. V., *Kinet. Katal.* **3,** 123 (1962).
2. Rubinshtein, A. M., Slinkin, A. A., and Pribytkova, N. A., *Izv. Akad. Nauk SSSR, Otd. Khim. Nauk* 814 (1958).
3. Rubinshtein, A. M., Akimov, V. A., and Kretalova, L. D., *Izv. Akad. Nauk SSSR, Otd. Khim. Nauk* 929 (1958).
4. Shalvoy, R. B., Reucroft, P. J., and Davis, B. H., *J. Vac. Sci. Technol.* **17,** 209 (1980).
5. Simonova, L. G., Dzisk'ko, V. A., Borisova, M. S., Karakchiev, L. G., and Olen'kova, I. P., *Kinet. Katal.* **14,** 1566 (1973).
6. Wu, M., and Hercules, D. M., *J. Phys. Chem.* **83,** 2003 (1979).
7. Vedrine, J. C., Hollinger, G., and Minh, O. T., *J. Phys. Chem.* **82,** 1515 (1978).
8. Bartholomew, C. H., and Ferranto, R. J., *J. Catal.* **45,** 41 (1976).
9. Cimino, A., and Schiavello, M., *J. Catal.* **20,** 202 (1971).
10. Ross, J. R. H., and Steel, M. C. F., *Trans. Faraday Soc.* **69,** 10 (1973).
11. Ross, J. R. H., Steel, M. C. F., and Zeini-Isfahani, A., *J. Catal.* **52,** 280 (1978).
12. Richardson, J. T., and Crump, J. G., *J. Catal.* **57,** 417 (1979).
13. "Catalyst Handbook." Wolfe Scientific Books, London, 1970.
14. Bartholomew, C. H., and Pannell, R. B., *J. Catal.* **65,** 390 (1980).
15. Klug, H. P., and Alexander, L. E., "X-Ray Diffraction Procedures." Wiley, New York, 1954.
16. Stokes, A. R., and Wilson, A. J. C., *Proc. Cambridge Philos. Soc.* **38,** 313 (1942).
17. Wertkeim, G. K., and Hufner, S., *Phys. Rev. Lett.* **28,** 1028 (1972).
18. Kim, K. S., and Davis, R. E., *J. Electron. Spectrosc.* **1,** 251 (1972).

19. Kim, K. S., and Winograd, W., *Surf. Sci.* **43,** 625 (1974).

20. Shalvoy, R. B., Reucroft, P. J., and Davis, B. H., *J. Catal.* **56,** 336 (1979).

21. Figlarz, M., Vincent, F., Lacaille, C., and Amiel, J., *Powder Technol.* **1,** 121 (1967).

22. Amelse, J. A., Arcuri, K. B., Butt, J. B., Matyl, R. J., Schwartz, L. H., and Shapiro, A., *J. Phys. Chem.* **85,** 708 (1981).

23. Wang, T., and Schmidt, L. D., *J. Catal.* **70,** 187 (1981).

24. Ruckenstein, E., and Chu, Y. F., *J. Catal.* **59,** 109 (1979).